Elegant Laguerre–Gaussian beams—formulation of exact vector solution

OPEN ACCESS
IOP Publishing
Journal of Optics
J. Opt. 20 (2018) 105601 (10pp)
https://doi.org/10.1088/2040-8986/aadc8a

Elegant Laguerre–Gaussian beams—formulation of exact vector solution

Wojciech Nasalski

Institute of Fundamental Technological Research, Polish Academy of Sciences, Pawińskiego 5b, 02-106 Warsaw, Poland

E-mail: wnasal@ippt.pan.pl

Received 3 May 2018, revised 10 August 2018
Accepted for publication 23 August 2018
Published 10 September 2018

Abstract

In photonic applications of optical beams, their transverse cross-section should be often narrow, with a diameter in their waist of the order of one wavelength or even less. Within this range, the paraxial approximation of beam fields is not valid and standard corrections by field expansions with respect to a small parameter are not efficient as well. Thus, still there is a need for more accurate beam field description. In this report, an exact vector solution for free-space propagation is given in terms of elegant Laguerre–Gaussian beams. The analysis starts from the known paraxial field approximation and next, through bidirectional field transformation and application of a Hertz potential leads to an exact vector solution. The role of the paraxial solution in construction of the exact solution is elucidated. The method works well not only in cases of free-space propagation but also in description of beam interactions with planar interfaces and multilayers.

Keywords: elegant Laguerre–Gaussian beams, paraxial and nonparaxial solutions, bidirectional transformation, Hertz potentials

(Some figures may appear in colour only in the online journal)

1. Introduction

Although the notion of elegant or complex-valued Gaussian beams was introduced by Siegman a long time ago [1, 2], they are still considered mostly as the scalar paraxial approximation of the Helmholtz equation solution. Their nonparaxial counterparts were mainly obtained in terms infinite series in powers of a small parameter yielding only successive corrections to the paraxial solutions [3, 4]. On the other hand, the set of the elegant Laguerre–Gaussian (eLG) beams of arbitrary order constitute a complete and biorthogonal base for electromagnetic fields, carry finite energy per unit length along their propagation direction and are expressed entirely by elementary functions. Their attractive properties, closely related to orbital angular momentum of light [5, 6], were demonstrated in the context of optical focusing, trapping and manipulations of nanoelements [7, 8].

Several nonparaxial attempts to treat exactly the beam propagation problem, based on the grounds of a scalar wave equation or on a full set of Maxwell's equations, were already reported, for example in [9–14] to name a few. Moreover, other different techniques, those based on Bessel functions or on nondiffractive beams, were reported as well [15–19]. In addition, an independent technique, which is based on a bidirectional transformation, was also presented in the past in constructions exact solutions to the propagation problem of localized electromagnetic pulses or focus wave modes [20–25]. After introducing some modifications and extensions to basics [20, 21] of this bidirectional technique, it is applied here in derivation of a new exact solution to the problem of beam propagation. It is stipulated that the beams are not accelerating. Note that the most reports mentioned above are of theoretical nature. Still, they show certain potential in considerations on recent progress in photonic technology [26–30].

In this paper, an exact bidirectional vortex beam solution is derived in an analytic closed form. Hertz potentials are created by direct use of eLG beams of arbitrary order. Starting points of this analysis are reports [31, 32] on paraxial beams and [33, 34] on nonparaxial beams. Beam propagation in free-space was

considered in [31–34], meanwhile both cases of normal and oblique incidence upon planar interfaces or multi-layered structures were accounted for in [31–33]. The beams are scaled in the transverse and longitudinal dimensions. Scalar, three-dimensional paraxial eLG beams are defined by applying complex derivatives [35] to the fundamental Gaussian. Their exact versions are obtained by creating separable beam solutions in the frame of bidirectional coordinates [36]. Next, from many available possibilities of using Hertz potentials [37], two of them, equal each other and oriented along the same direction of beam propagation, are chosen in construction exact vector components of the eLG beam.

Finally, the electromagnetic field of the exact vector eLG solution is obtained in a square-integrated form of finite power flow. The solution is complete and expressed only by standard elementary functions, without the need of referring to any approximation or infinite field expansion. Each one from its transverse magnetic (TM) or transverse electric (TE) solutions comprises two transverse and one longitudinal mutually orthogonal eLG beam ingredients. Their amplitudes are distinguished uniquely by the ratio of the transverse and longitudinal field scales. The solution is exact but still in phase front planes of the exact eLG beams they replicate the standard paraxial eLG beams. In the case of incidence on planar layered structures, the transverse field components satisfy a transmission matrix equation specified by Fresnel coefficients of the scattering structure. Thus, the solutions obtained are valid not only for the description of beam propagation in free-space, but also for the analysis of beam interactions with planar interfaces or multilayers, including both cases of normal and oblique beam incidence. To the best of the author's knowledge, the solution presented here is new.

The paper is organized as follows. After a short introduction given in section 1, coordinate scaled notations are specified in section 2. Scalar eLG paraxial beams are described in real and complex variables in sections 3 and 4, respectively. Scalar and vector exact eLG beams are defined by the bidirectional transformation in section 5 and by use of the Hertz potential in section 6, respectively. In section 7, the analysis of beam-interface interactions is presented and illustrated by results of numerical simulations. Finally, the main characteristics of the eLG beam solutions obtained are summarized in section 8.

2. Notation and scaling

In this analysis, the spatial variables x, y and their momentum counterparts k_x, k_y transverse to the z-axis of beam propagation direction are scaled by a transverse scaling parameter—a cross-section radius or half-width w_w of a cylindrically symmetric beam placed at its waist plane $z = 0$:

$$x/w_w \to x,\ \ k_x w_w \to k_x, \tag{1a}$$

$$y/w_w \to y,\ \ k_y w_w \to k_y. \tag{1b}$$

Similarly, using a diffraction length $z_D = kw_w^2$, the spatial variables z, ct and their longitudinal counterparts—wave number k and frequency $\omega = kc$ are scaled by z_D:

$$z/z_D \to z,\ \ kz_D \to k, \tag{2a}$$

$$ct/z_D \to ct,\ \omega z_D \to \omega, \tag{2b}$$

where t is time, c is speed of light and $z_D^2/w_w^2 \to k$ on the grounds of (2a). The scales w_w and z_D specify a paraxial parameter:

$$f = 2^{-1/2} w_w/z_D = 2^{-1/2}(kw_w)^{-1} \to (2k)^{-1/2}, \tag{2c}$$

small for wide (paraxial) beams and large for narrow (non-paraxial) beams. As was shown in [33, 34], this parameter distinguishes between two beam field ingredients which appear in the exact vector beam field solution.

Optical beams will be considered monochromatic $\propto e^{-ikct}$ and propagating, unless otherwise stated, in a linear, transparent, isotropic and homogeneous medium specified by its characteristic admittance Y and impedance Z. However, after normalization of electromagnetic field:

$$\boldsymbol{E}\sqrt{Y} \to \boldsymbol{E},\ \ \boldsymbol{H}\sqrt{Z} \to \boldsymbol{H} \tag{3}$$

the beams will be understood as propagating in free-space. Note that the scaling changes a form of wave equations. For example, an amplitude U of a scalar beam field $V = Ue^{-ikct}$ will be governed by the scaled Helmholtz equation:

$$[(w_w/z_D)^2(k^2 + \partial_z^2) + \partial_x^2 + \partial_y^2]\, U(x, y, z) = 0. \tag{4}$$

In the following, the Cartesian $(\hat{\boldsymbol{e}}_x, \hat{\boldsymbol{e}}_y, \hat{\boldsymbol{e}}_z)$, cylindrical $(\hat{\boldsymbol{e}}_\rho, \hat{\boldsymbol{e}}_\varphi, \hat{\boldsymbol{e}}_z)$ and circular $(\hat{\boldsymbol{e}}_R, \hat{\boldsymbol{e}}_L, \hat{\boldsymbol{e}}_z)$ polarization frames will be interchangeably used.

3. Scalar paraxial eLG beams in real coordinates

Let us start with the eLG beam $G_{p,\pm l}$ as solution to the paraxial (Fock) equation:

$$\left[i\partial_z + \tfrac{1}{2}(\partial_x^2 + \partial_y^2)\right] G_{p,\pm l}(x, y, z) = 0. \tag{5}$$

The beam is labeled by radial p and azimuthal $\pm l$ indices, where p and l are non-negative integers. The 'upper' and 'lower' signs in $\pm l$ indicate the right-handed and left-handed orbital angular momentum of beam vortices, respectively. This solution is expressed by the product:

$$G_{p,\pm l}(x, y, z) = Q_{p,l}(x, y, z)\, e^{\pm il\phi} \tag{6a}$$

of a vortex phase factor $e^{\pm il\phi}$ and a beam field envelope

$$Q_{p,l}(x, y, z) = (-1)^{p+l} v^{-(2p+l)}\, u^l\, L_p^l(u^2)\, g(x, y, z). \tag{6b}$$

In spite of the presence in (6b) the beam complex radius scaled $v(z) = (1 + iz)^{1/2}$ the beam envelope depends only on the complex argument

$$u(x, y, z) = 2^{-1/2} r_\perp(x, y) v^{-1}(z), \tag{7}$$

$r_\perp = (x^2 + y^2)^{1/2}$, present in $Q_{p,l}$ through its powers u^l, the fundamental Gaussian beam

$$g(x, y, z) = v^{-2}(z) \exp[-u^2(x, y, z)] \tag{8}$$

and the associated Laguerre polynomials with biorthogonal property:

$$L_p^l(u^2) = u^{-2l}e^{u^2}(d/du^2)^p e^{-u^2}u^{2(p+l)}, \tag{9a}$$

$$\int_0^\infty e^{-u^2}u^{2l}L_p^l(u^2)L_q^l(u^2)du^2 = p!(p+l)!\delta_{pq}, \tag{9b}$$

where $L_0^l(u^2) = 1$, $L_1^l(u^2) = -u^2 + l + 1$ and so on. The beam complex radius $v(z)$ is the only quantity in the beam field solution (6)–(9) which depends on z. It defines, through the relation

$$v^{-2}(z) = w^{-2}(z) - iR^{-1}(z) = (1 - iz)(1 + z^2)^{-1}, \tag{10}$$

changes of the beam radius w and the phase front curvature R appearing in the course of beam propagation along the z-axis. Contrary to the vortex factor $e^{\pm il\varphi}$, the beam envelope $Q_{p,l}$ does not depend on signs of the azimuthal index $\pm l$ or of the azimuthal angle $\pm\varphi$. The amplitude normalization of all the eLG functions is introduced by the condition $g = 1$ imposed on the Gaussian beam field amplitude at the centre of its waist plane.

4. Scalar paraxial eLG beams in complex coordinates

On the other hand, there exists another, although completely equivalent, definition of the eLG paraxial beams [31]. This definition seems to be more suitable in further analysis of the problem. Let us introduce new complex coordinates with single vortex factors $e^{\pm i\phi}$ and $e^{\pm i\varphi}$ explicitly present in their definitions in the configuration and momentum domains, respectively:

$$\begin{aligned} \varsigma_\pm &= 2^{-1/2}(x \pm iy) = \varsigma_\perp e^{\pm i\phi}, \\ \kappa_\pm &= 2^{-1/2}(k_x \pm ik_y) = \kappa_\perp e^{\pm i\varphi}, \end{aligned} \tag{11}$$

where $\varsigma_\perp = 2^{-1/2}r_\perp$, $\kappa_\perp = 2^{-1/2}k_\perp$, $r_\perp^2 = x^2 + y^2$, $k_\perp^2 = k_x^2 + k_y^2$, $\tan\phi = y/x$ and $\tan\varphi = k_y/k_x$. In these new coordinates Helmholtz and Fock equations read:

$$[(w_w/z_D)^2(k^2 + \partial_z^2) + 2\partial_{\varsigma_+}\partial_{\varsigma_-}]\, G_{p,\pm l}(\varsigma_+, \varsigma_-, z)e^{ikz} = 0, \tag{12}$$

$$(i\partial_z + \partial_{\varsigma_+}\partial_{\varsigma_-})G_{p,\pm l}(\varsigma_+, \varsigma_-, z) = 0. \tag{13}$$

Note that the same notation is used for functions dependent on ς_+ and ς_- instead of x and y. The Gaussian beam $g = v^{-2}e^{-u^2}$ is still defined in (8) by the substitution $u^2 = \varsigma_\perp^2 v^{-2}$.

The eLG beams of higher orders $2p + l \neq 0$ are defined by $2p + l$ derivatives of $g \equiv G_{0,0}$:

$$G_{p,\pm l}(\varsigma_+, \varsigma_-, z) = \partial_{\varsigma_\pm}^p \partial_{\varsigma_\mp}^{p+l} g(\varsigma_+, \varsigma_-, z), \tag{14a}$$

$$Q_{p,l}(\varsigma_+, \varsigma_-, z) = \partial_{\varsigma_\perp}^{2p+l} g(\varsigma_+, \varsigma_-, z). \tag{14b}$$

These definitions of the eLG beam $G_{p,\pm l}$ and its envelope $Q_{p,l} = G_{p,\pm l}e^{\mp il\phi}$ are equivalent to those given in (5) and (6). The derivatives $\partial_{\varsigma_\pm} = e^{\mp i\phi}\partial_{\varsigma_\perp}$ applied to $G_{p,\pm l}$ of the order $2p + l$ create new eLG beams with their order increased to $2p + l + 1$:

$$\partial_{\varsigma_\pm}G_{p,\pm l} = G_{p+1,\pm(l-1)}, \;\; \partial_{\varsigma_\mp}G_{p,\pm l} = G_{p,\pm(l+1)}. \tag{15}$$

Further, $\partial_{\varsigma_+}\partial_{\varsigma_-}G_{p,\pm l} = G_{p+1,\pm l}$ creates new eLG beam of the order $2p + l + 2$ and so on. Moreover, through the Fourier transform:

$$\begin{aligned} &G_{p,\pm l}(\varsigma_+, \varsigma_-, z_+) \\ &\quad = \tfrac{i}{2\pi}\int d\kappa_+ d\kappa_- \tilde{G}_{p,\pm l}(\kappa_+, \kappa_-, z_+)e^{+i(\kappa_+\varsigma_- + \kappa_-\varsigma_+)}, \end{aligned} \tag{16a}$$

$$\begin{aligned} &\tilde{G}_{p,\pm l}(\kappa_+, \kappa_-, z_+) \\ &\quad = \tfrac{i}{2\pi}\int d\varsigma_+ d\varsigma_- G_{p,\pm l}(\varsigma_+, \varsigma_-, z_+)e^{-i(\kappa_+\varsigma_- + \kappa_-\varsigma_+)}, \end{aligned} \tag{16b}$$

the solution $\tilde{G}_{p,\pm l}$ in the momentum or spatially spectral domain is given by:

$$\tilde{G}_{p,\pm l}(\kappa_+, \kappa_-, z) = (i)^{2p+l}\kappa_\mp^p \kappa_\pm^{p+l}\tilde{g}(\kappa_+, \kappa_-, z), \tag{17a}$$

$$\tilde{Q}_{p,l}(\kappa_+, \kappa_-, z) = (i\kappa_\perp)^{2p+l}\tilde{g}(\kappa_+, \kappa_-, z), \tag{17b}$$

with the Fourier transformed beam envelope $\tilde{Q}_{p,l} = \tilde{G}_{p,\pm l}e^{\mp il\phi}$ and Gaussian beam $\tilde{g} = e^{-\kappa_\perp^2 v^2}$. Note that the definitions (17) are valid not only for positive but also for fractional or even negative values of the radial index p.

In addition to the creation new eLG beams of higher orders shown in (15), the multiplication them by vortex factors $e^{\pm i\phi}$ and $e^{\pm 2i\varphi}$ also creates new eLG beams but this time of the same order [31]. The definition (14) implies in the configuration domain:

$$G_{p,\pm l} = G_{p+1,\pm(l-2)}e^{\pm 2i\phi}, \;\; G_{p,\pm l} = G_{p-1,\pm(l+2)}e^{\mp 2i\phi}, \tag{18a}$$

$$G_{p,\pm l} = G_{p+1/2,\pm(l-1)}e^{\pm i\phi}, \;\; G_{p,\pm l} = G_{p-1/2,\pm(l+1)}e^{\mp i\phi}. \tag{18b}$$

In the momentum domain, identities equivalent to (18) are obtained for the Fourier transformed eLG beams defined in (17). That implies substitution in (18) the terms $G_{p,\pm l}$ and ϕ for $\tilde{G}_{p,\pm l}$ and φ, respectively. The interesting case in (18) seems this where the radial index changes its sign. For example, for $p = 0$ and $l = 1$ the identities of (18a) read:

$$G_{0,+1} = G_{1,-1}e^{+2i\phi}, \;\; G_{0,+1} = G_{-1,+3}e^{-2i\phi}, \tag{19a}$$

$$G_{0,-1} = G_{1,+1}e^{-2i\phi}, \;\; G_{0,-1} = G_{-1,-3}e^{+2i\phi}. \tag{19b}$$

These cases will be discussed more deeply in section 7. Note that identities (18) and (19) are equally valid for paraxial and nonparaxial eLG beams.

The identities (18) and (19) describe the effects of interactions between eLG beam fields and additional vortices nested in them. They are particularly suitable in considerations on solutions of beam propagation in free-space as well as on beam interactions with interfaces or multilayers. Note that the identities (18) follow exactly the original relations (10) and (11) given in [34] in the momentum domain. Contrary to what I previously suggested in the Erratum to [34], all the relations, (10) and (11) given in [34] and (18a) and (18b) presented here, are valid and sufficient in derivations of the solutions considered in this paper for positive as well as for negative values of the beam field topological charges $\pm l$.

5. Scalar exact eLG beams

The scalar eLG solution presented in section 4 is valid only for paraxial beams. But still, an exact version of this solution can be obtained as well by bidirectional modification of this solution. To this end, let us start, per analogy to the problem discussed in [36], with the transform of the coordinates z and ct into the new bidirectional coordinates z_- and z_+:

$$z_- = z - ct,\ z_+ = z + ct. \tag{20}$$

The first definition in (20) just rewrites the common propagation factor $e^{ikz_-} = e^{ik(z-ct)}$ in the new coordinate z_- and indicates, as usual, that the beam phase front at $z_- = 0$ propagates along the beam axis with speed of light. However, the replacement of z by the second new coordinate z_+ in the beam envelope $Q_{p,l}$ results in the propagation of this envelope in the backward direction of the beam axis, also with speed of light. These presumptions result in the new beam field solutions expressed by z_+ and z_-, instead of z and ct:

$$V(\varsigma_+, \varsigma_-, z_+, z_-) = G_{p,\pm l}(\varsigma_+, \varsigma_-, z_+)e^{ikz_-}, \tag{21}$$

$$G_{p,\pm l}(\varsigma_+, \varsigma_-, z_+) = Q_{p,l}(\varsigma_+, \varsigma_-, z_+)e^{\pm il\phi}, \tag{22}$$

together with a new definition of the complex radius squared of the beam field envelope:

$$v(z_+) = (1 + iz_+/2)^{1/2}. \tag{23}$$

The new field solution is governed exactly, without any (paraxial) approximation, by the scalar wave and Fock equations:

$$[2(w_w/z_D)^2\partial_{z_+}\partial_{z_-} + \partial_{\varsigma_+}\partial_{\varsigma_-}]V(\varsigma_+, \varsigma_-, z_+, z_-) = 0, \tag{24}$$

$$(2i\partial_{z_+} + \partial_{\varsigma_+}\partial_{\varsigma_-})G_{p,\pm l}(\varsigma_+, \varsigma_-, z_+) = 0. \tag{25}$$

All of that results in the bidirectional exact extension of the previously paraxial approximation of the wave equation. The monochromatic field V expressed by (21) and the eLG beam field $G_{p,\pm l}$ expressed by (22) are now exact solutions to both wave equation (24) and Fock equation (25), respectively. Note that the ansatz $z,\ ct \to z_-,\ z_+$ applied in equations (21)–(25) is in the order opposite to that of $z,\ ct \to z_+,\ z_-$ applied in the derivation of focus wave modes [20–23].

Let us look closer into the main features of this exact solution. A boundary value problem is assumed here at the moment $ct = 0$ and at the waist plane $z_+ = z_- = z = 0$:

$$V(\varsigma_+, \varsigma_-, 0, 0) = G_{p,\pm l}(\varsigma_+, \varsigma_-, 0). \tag{26}$$

This condition is exactly the same in its form as that for the approximate paraxial solution. Moreover, for $ct \neq 0$, although the beam phase front plane is placed, as it was in the paraxial case, at $z_- = z - ct = 0$, the position of the beam waist plane now is not constant, but is moving backward to its new position at $z_+ = z + ct = 0$. Therefore, these two planes are moving in the opposite directions along the z-axis and the distance between them is always $2z$. At the phase front plane defined by $z_- = 0$ and $z_+ = 2z$ the beam radius (24) of the exact solution is given by

$$v(z_+) = (1 + iz_+/2)^{1/2} = (1 + iz)^{1/2} = v(z), \tag{27}$$

what exactly is the radius of the paraxial beam. Thus, at the waist or phase front planes, the exact solution $G_{p,\pm l}(\varsigma_+, \varsigma_-, 2z)$ to exact Fock equation (22) duplicates the paraxial solution $G_{p,\pm l}(\varsigma_+, \varsigma_-, z)$ to approximate Fock equation (13). In other words, at phase front planes of the beams, the exact scalar eLG solution reduces to the well known paraxial scalar eLG solution.

6. Vector exact eLG beams

In section 5, the derivation route from the paraxial scalar eLG beam solution to its exact scalar version was presented. However, the exact vector beam solution should satisfy a full set of Maxwell's equations:

$$\partial_{ct}\boldsymbol{H} = -(z_D/w_w)\nabla \times \boldsymbol{E},\ \partial_{ct}\boldsymbol{E} = (z_D/w_w)\nabla \times \boldsymbol{H}, \tag{28a}$$

$$\nabla \cdot \boldsymbol{H} = 0,\ \nabla \cdot \boldsymbol{E} = 0, \tag{28b}$$

with $\nabla = \hat{\boldsymbol{e}}_x\partial_x + \hat{\boldsymbol{e}}_y\partial_y + (w_w/z_D)\hat{\boldsymbol{e}}_z\partial_z$, where $\partial_z = \partial_{z_+} + \partial_{z_-}$ and $\partial_{ct} = \partial_{z_+} - \partial_{z_-}$. It is well known that such solution can be constructed from two vector Hertz potentials, say $\boldsymbol{M}$ and $\boldsymbol{N}$ [37]. Among many other possibilities, both of them are assumed here as directed along their beam axes, equal each other $\boldsymbol{M} = \boldsymbol{N} = (0, 0, M_z)$ and expressed by one longitudinal eLG component:

$$M_z(\varsigma_+, \varsigma_-, z_+, z_-) = w_w^2 G_{p,\pm l}(\varsigma_+, \varsigma_-, z_+)e^{ikz_-}. \tag{29}$$

That specifies the following beam field compositions:

$$\begin{aligned}\boldsymbol{E} &= \boldsymbol{E}^{(tm)} + \boldsymbol{E}^{(te)}\\ &= \nabla \times \nabla \times \hat{\boldsymbol{e}}_z M_z - (w_w/z_D)\partial_{ct}\nabla \times \hat{\boldsymbol{e}}_z M_z,\end{aligned} \tag{30a}$$

$$\begin{aligned}\boldsymbol{H} &= \boldsymbol{H}^{(te)} + \boldsymbol{H}^{(tm)}\\ &= \nabla \times \nabla \times \hat{\boldsymbol{e}}_z M_z + (w_w/z_D)\partial_{ct}\nabla \times \hat{\boldsymbol{e}}_z M_z.\end{aligned} \tag{30b}$$

In the circular frame $(\hat{\boldsymbol{e}}_R, \hat{\boldsymbol{e}}_L, \hat{\boldsymbol{e}}_z)$, these compositions read [34]:

$$\boldsymbol{E}^{(tm)} = (w_w/z_D)(\hat{\boldsymbol{e}}_R\partial_{\varsigma_+} + \hat{\boldsymbol{e}}_L\partial_{\varsigma_-})\partial_z M_z - 2\hat{\boldsymbol{e}}_z\partial_{\varsigma_+}\partial_{\varsigma_-}M_z, \tag{31a}$$

$$\boldsymbol{E}^{(te)} = -i(w_w/z_D)(\hat{\boldsymbol{e}}_R\partial_{\varsigma_+} - \hat{\boldsymbol{e}}_L\partial_{\varsigma_-})\partial_{ct}M_z \tag{31b}$$

with the magnetic field given from the duality principle. Application of the beam definitions presented in section 4 and the relations between transverse (polar) parts of the cylindrical and circular polarization frames:

$$\hat{\boldsymbol{e}}_R = 2^{-1/2}(\hat{\boldsymbol{e}}_\rho + i\hat{\boldsymbol{e}}_\phi)\, e^{+i\phi},\ \hat{\boldsymbol{e}}_L = 2^{-1/2}(\hat{\boldsymbol{e}}_\rho - i\hat{\boldsymbol{e}}_\phi)\, e^{-i\phi}, \tag{32}$$

$\rho = r_\perp$, leads, after some straightforward algebra, to the TM and TE vector solutions expressed by the eLG beams $G_{p,\pm(l+1)}$, $G_{p+1,\pm(l+1)}$, $G_{p+1,\pm l}$, vortex factors $e^{\mp il\varphi}$ and the paraxial parameter f defined in (2c). In the polarization frame $(\hat{\boldsymbol{e}}_\rho, \hat{\boldsymbol{e}}_\phi, \hat{\boldsymbol{e}}_z)$, $\rho = r_\perp$, this solution reads:

$$\begin{aligned}\boldsymbol{E}^{(tm)}_{p,\pm l} = {} & i\hat{\boldsymbol{e}}_\rho(f^{-1}G_{p,\pm(l+1)} + f^{+1}G_{p+1,\pm(l+1)})e^{\mp i\phi}e^{ikz_-}\\ & - 2\hat{\boldsymbol{e}}_z G_{p+1,\pm l}\, e^{ikz_-},\end{aligned} \tag{33a}$$

$$\boldsymbol{E}^{(te)}_{p,\pm l} = i\hat{\boldsymbol{e}}_\phi(f^{-1}G_{p,\pm(l+1)} - f^{+1}G_{p+1,\pm(l+1)})e^{\mp i\phi}e^{ikz_-}, \tag{33b}$$

with its transverse $\boldsymbol{E}^{(tm)}_{\perp;p,\pm l}$, $\boldsymbol{E}^{(te)}_{\perp;p,\pm l}$ and longitudinal $\boldsymbol{E}^{(tm)}_{z;p,\pm l}$ field components. Meanwhile, both transverse and longitudinal field components possess the same topological charge equal $\pm l$, the charges attributed only to the eLG beams in the transverse TM or TE fields equal $\pm(l+1)$ and are larger or smaller by one than that of the longitudinal beam component. As expected, divergence of all these field solutions is null. In spite of the opposite sign in amplitudes in the TE solution, the difference between the eLG beams in the paraxial and nonparaxial parts of the solution reduces only to the increment of the radial index by one.

In solution (33), three mutually orthogonal exact scalar eLG beams of different mode orders contribute separately to the transverse and longitudinal components of the vector eLG beam. Positions of their phase front and waist planes are specified by zeroes of the bidirectional longitudinal coordinates z_- and z_+, respectively. The impact of beam propagation on the beam spatial shape is specified completely by values of the beam complex radius v dependent only on z_+ as shown in (27). The longitudinal TM field component $-2G_{p+1,\pm l}$ does not depend on the paraxial parameter f. On the contrary, each transverse field component of TM or TE polarization consists of two mutually independent—paraxial $f^{-1}G_{p,\pm(l+1)}ie^{\mp i\phi}$ and nonparaxial $f^{+1}G_{p+1,\pm(l+1)}ie^{\mp i\phi}$—ingredients, with their amplitudes specified by the paraxial parameter f and phase shifted by $ie^{\mp i\phi}$. All field components possess their topological charge $\pm l$ attributed to the same vortex factor $e^{\mp il\phi}$. For small or large values of f, the transverse parts of the exact beam field solution correspond to the paraxial or nonparaxial parts of this solution, respectively.

Equivalent solution in the circular polarization frame is given by use of (32) in the field expressions (33). For the right-handed vortex $e^{+il\phi}$ nested in the beam field, the solution reads, for the TM field:

$$\begin{aligned}\boldsymbol{E}^{(tm)}_{p,+l} &= (\hat{\boldsymbol{e}}_R G^{(tm)}_{R;p,l} + \hat{\boldsymbol{e}}_L G^{(tm)}_{L;p,l} + \hat{\boldsymbol{e}}_z G^{(tm)}_{z;p,l})\, e^{ikz_-} \\ &= (\boldsymbol{E}^{(tm)}_{\perp;p,l} + \hat{\boldsymbol{e}}_z G^{(tm)}_{z;p,l})\, e^{ikz_-}, \qquad (34a)\end{aligned}$$

$$G^{(tm)}_{R;p,l} = i\,2^{-1/2}(f^{-1}G_{p+1,l-1} + f^{+1}G_{p+2,l-1}), \qquad (34b)$$

$$G^{(tm)}_{L;p,l} = i\,2^{-1/2}(f^{-1}G_{p,l+1} + f^{+1}G_{p+1,l+1}), \qquad (34c)$$

$$G^{(tm)}_{z;p,l} = -2\,G_{p+1,+l} \qquad (34d)$$

and for the TE field:

$$\boldsymbol{E}^{(te)}_{p,+l} = (\hat{\boldsymbol{e}}_R G^{(te)}_{R;p,l} + \hat{\boldsymbol{e}}_L G^{(te)}_{L;p,l})\, e^{ikz_-} = \boldsymbol{E}^{(te)}_{\perp;p,l} e^{ikz_-}, \qquad (35a)$$

$$G^{(te)}_{R;p,l} = -2^{-1/2}(f^{-1}G_{p+1,l-1} - f^{+1}G_{p+2,l-1}), \qquad (35b)$$

$$G^{(te)}_{L;p,l} = +2^{-1/2}(f^{-1}G_{p,l+1} - f^{+1}G_{p+1,l+1}). \qquad (35c)$$

The solutions $\boldsymbol{E}^{(tm)}_{p,-l}$ and $\boldsymbol{E}^{(te)}_{p,-l}$ for the left-handed vortex $e^{-il\phi}$ can be derived per analogy or obtained by the direct substitutions in (34) and (35): $l \to -l$, $l+1 \to -l-1$, $l-1 \to -l+1$ and with $\hat{\boldsymbol{e}}_R, \hat{\boldsymbol{e}}_L \to \hat{\boldsymbol{e}}_L, \hat{\boldsymbol{e}}_R$ for TM polarization (34) and $\hat{\boldsymbol{e}}_R, \hat{\boldsymbol{e}}_L \to -\hat{\boldsymbol{e}}_L, -\hat{\boldsymbol{e}}_R$ for TE polarization (35) [33].

Expressions (33)–(35) of the exact solution to the eLG beam propagation problem discussed here represent the main result of the paper. It is evident that in any polarization frame the three eLG beams $G_{p,\pm(l+1)}$, $G_{p+1,\pm(l+1)}$ and $G_{p+1,\pm l}$, together with additional vortex factors $e^{\mp i\phi}$, or the other eLG beams of the same order obtained from them by identities (18), are building blocks of paraxial, nonparaxial and longitudinal parts of the exact vector eLG beam solution, respectively. Note that, in spite of their names, these parts of the total exact solution are also exact. Owing to completeness and biorthogonal features of these beams, their compositions span the whole space of physically accessible modes of finite power flux for free-space propagation. Moreover, it appears that the same set of the eLG beams defines also normal modes of planar interfaces or multilayers of the hosting medium [31, 32]. This will be shown in the next section.

7. ELG beams at planar interfaces

Let us consider now the canonical problem of beam interaction with a planar interface between two semi-infinite isotropic and homogeneous media. The interface is assumed transverse to the incident beam propagation direction along the beam axis and is specified in the momentum domain by Fresnel transmission t_p and t_s coefficients for TM and TE polarization, respectively. The parameters t_p and t_s are dispersive as they depend on the ratio $\eta = \cos\theta_2 / \cos\theta_1$ of cosines of refraction and incidence angles θ_2 and θ_1, respectively. Meanwhile the longitudinal field component $\hat{\boldsymbol{e}}_z \tilde{G}^{(tm)}_{z;p,l}$ is always continuous at the interface, the transverse field components are eigenfunctions of a transmission matrix $\boldsymbol{T}$ separately for paraxial and nonparaxial parts of the eLG beam fields defined in (33)–(35). In the transverse circular polarization frame $(\hat{\boldsymbol{e}}_R, \hat{\boldsymbol{e}}_L)$, the transmission matrix $\boldsymbol{T} = \boldsymbol{T}_{(R,L)}$ is composed of diagonal and antidiagonal parts with amplitude factors equal to $\frac{1}{2}(\eta t_p + t_s)$ and $\frac{1}{2}(\eta t_p - t_s)$, respectively [31]:

$$\boldsymbol{T}_{(R,L)} = \tfrac{1}{2}(\eta t_p + t_s)\begin{bmatrix}1 & 0\\ 0 & 1\end{bmatrix} + \tfrac{1}{2}(\eta t_p - t_s)\begin{bmatrix}0 & e^{-2i\varphi}\\ e^{+2i\varphi} & 0\end{bmatrix}. \qquad (36)$$

The second term of this matrix implies excitation of the eLG beam with polarization orthogonal to that of the incident eLG beam, with the beam amplitude multiplied by the factor $\frac{1}{2}(\eta t_p - t_s)$ and with the radial p and azimuthal l indices changed by ∓ 1 and ± 2, respectively. This effect of the cross-polarization coupling between orthogonal transverse beam components disappears for normal incidence in the momentum domain, that is where $\eta t_p - t_s = 0$.

Let us turn for a while to the eLG beams defined by (14) in the configuration domain. For brevity of presentation, we consider here the incident beam field as only one ingredient of the transverse field $\boldsymbol{E}^{(tm)}_{\perp,p,\pm l}$ defined in (34) and (35). Consider the beam $\hat{\boldsymbol{e}}_L G_{0,1}$ of left-handed circular polarization incident normally on the interface. The beam waist plane coincides with the interface. Then, according to the transfer matrix $\boldsymbol{T}_{(R,L)}$ form, two beams are excited below the interface, the first one of the left-handed and the second one of the right-handed polarizations, respectively:

$$G_{0,+1} = -\tfrac{1}{\sqrt{2}} r_\perp e^{-\frac{1}{2}r_\perp^2 + i\phi},\quad G_{1,-1} = \tfrac{1}{2\sqrt{2}} r_\perp (4 - r_\perp^2)\, e^{-\frac{1}{2}r_\perp^2 - i\phi}. \qquad (37)$$

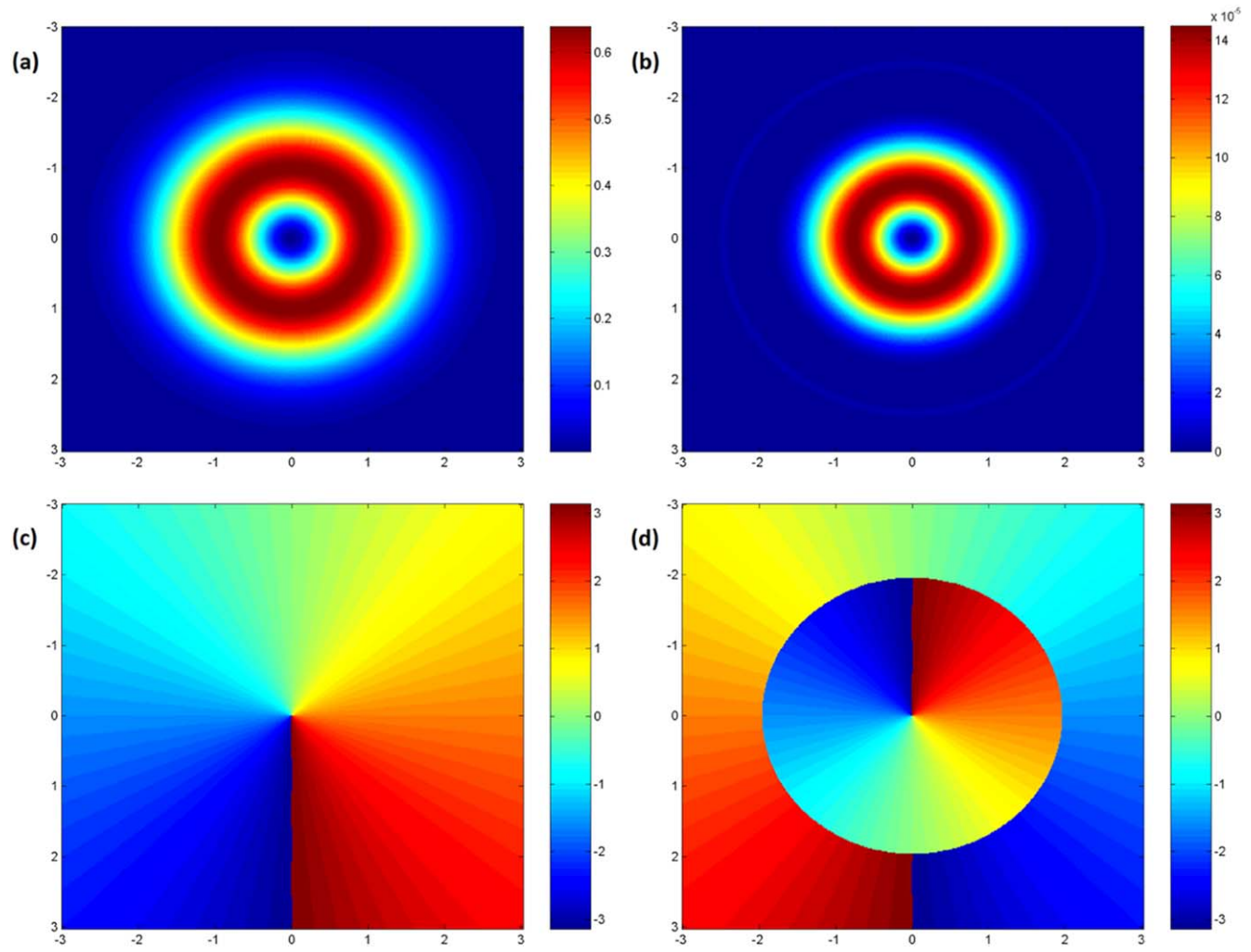

Figure 1. Intensities (a), (b) and phases (c), (d) of beam fields excited at the interface: $\hat{\boldsymbol{e}}_L G_{0,1}$ in (a), (c) and $\hat{\boldsymbol{e}}_R G_{1,-1}$ in (b), (d). Normal incidence of the beam $\hat{\boldsymbol{e}}_L G_{0,1}$ of left-handed circular polarization, fields shown in the configuration domain in the frame (x, y).

In addition, modifications of the beam field distributions (37) come from the amplitude factors $\frac{1}{2}(\eta t_p \pm t_s)$ present in $\boldsymbol{T}_{(R,L)}$. The case of external reflection is considered here with the contrast of refraction indices equal to 1.5. The radius w_w of the incident beam waist is equal to one wavelength. In this case, the field intensity modifications due to the dispersion of the coefficients t_p and t_s still are not strongly significant. For comparison with theoretical predictions and by analogy to the analysis presented in [31], a few examples of eLG beam field distribution are presented below.

Results of numerical simulation of transmitted fields excited at the interface by incidence of the beam $\hat{\boldsymbol{e}}_L G_{0,1}$ are presented in figure 1 in the configuration domain. This incidence deserves attention because it shows reverse of the sense of phase rotation under the beam interaction with the interface.

The field intensity distributions of $G_{0,1}$ and $G_{1,-1}$ beams shown in figures 1(a) and (b), follow closely their definitions given in (37), respectively. Moreover, the beam phase distributions shown in figures 1(c) and (d) are exactly specified by these definitions. The topological charges or azimuthal indices of beams are equal to $+1$ in figure 1(c) for the transmitted beam $\hat{\boldsymbol{e}}_L G_{0,1}$ and to -1 in figure 1(d) for the transmitted beam $\hat{\boldsymbol{e}}_R G_{1,-1}$. Their radial indices are equal to 0 in figure 1(c) for the beam $\hat{\boldsymbol{e}}_L G_{0,1}$ and to 1 in figure 1(d) for the beam $\hat{\boldsymbol{e}}_R G_{1,-1}$. The direction of the phase winding rotation is reversed and the global phase change by π is present between the beams $G_{0,1}$ and $G_{1,-1}$. Moreover, the phase changes by π are also present for the beam $G_{1,-1}$ at points of the circle of $r_\perp$ equal close to 2, as shown in figure 1(d).

The analogical case of incidence $\hat{\boldsymbol{e}}_R G_{0,1}$ is presented in figure 2. Similarly to what was presented in figure 1, the field intensity distributions shown in figures 2(a) and (b) follow also the definitions (37) of $G_{0,1}$ and $G_{-1,3}$, respectively. However, the sense of the phase rotation presented in figure 2(d) for the beam $\hat{\boldsymbol{e}}_L G_{-1,3}$ is the opposite to that what was presented in figure 1(d) for the beam $\hat{\boldsymbol{e}}_R G_{1,-1}$. That means that the phase rotation of the transmitted beam is of the same direction as for the incident beam $\hat{\boldsymbol{e}}_L G_{0,1}$. No phase changes by π are visible. Instead, there is the increase of the topological charge value l from one to three, that is the change from $\hat{\boldsymbol{e}}_L G_{0,1}$ to $\hat{\boldsymbol{e}}_R G_{-1,3}$.

In the numerical simulations presented above, only one beam $G_{0,1}$ of circular polarization—left-handed or right-handed

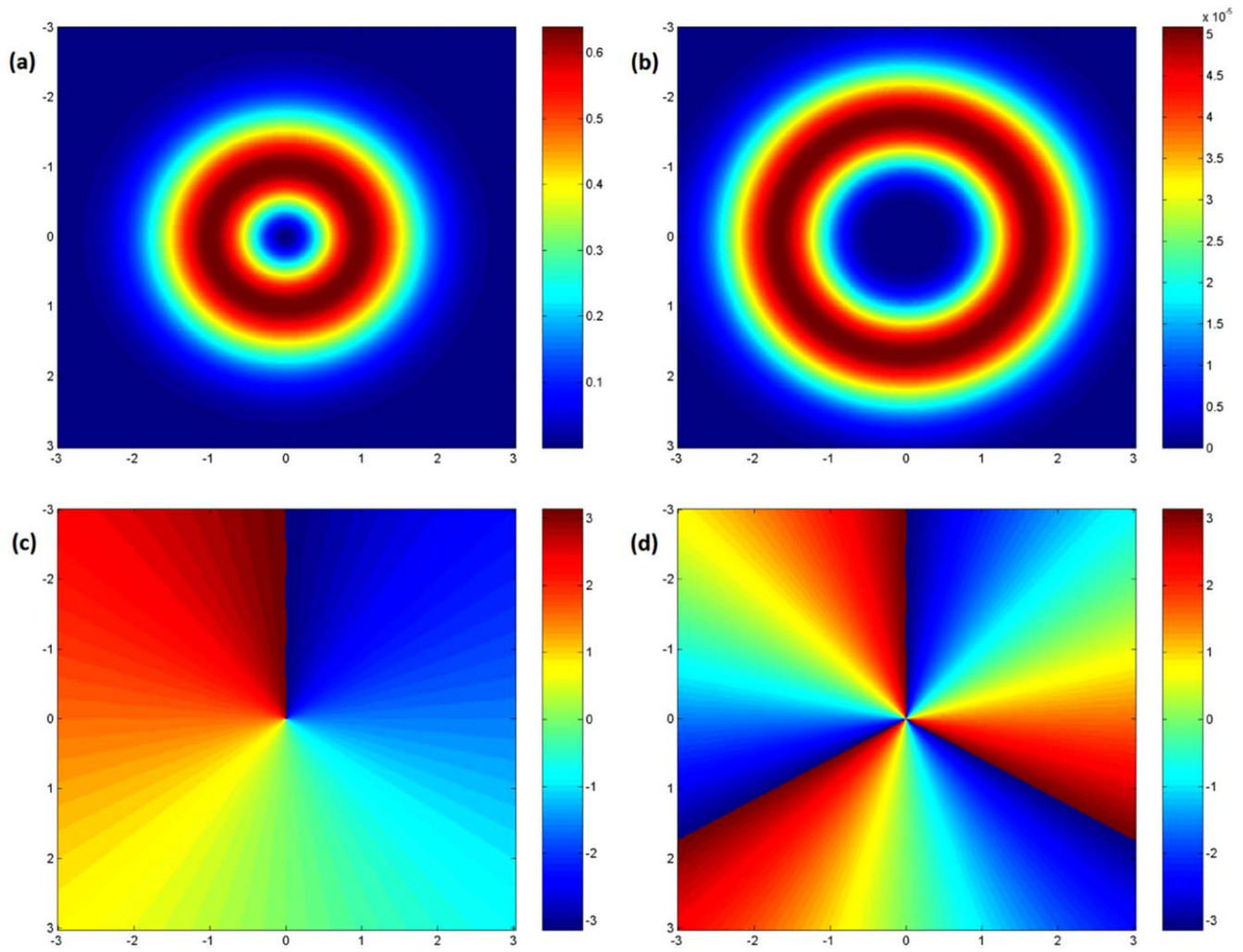

Figure 2. Intensities (a), (b) and phases (c), (d) of beam fields excited at the interface: $\hat{\boldsymbol{e}}_L G_{0,1}$ in (a), (c) and $\hat{\boldsymbol{e}}_L G_{-1,3}$ in (b), (d). Normal incidence of the beam $\hat{\boldsymbol{e}}_R G_{0,1}$ of right-handed circular polarization, fields shown in the configuration domain in the frame (x, y).

—is incident upon the interface and excites two transmitted field components of the circular polarization. However, on the grounds of the transmission matrix form (36) and the identities (18*a*), all of these beam field components belong to the same transverse TM beam field mode $\tilde{\boldsymbol{E}}^{(tm)}_{\perp;p,\pm l}$ defined in (34) by the same values of p and $\pm l$. Therefore, this beam field vector is the eigenvector of the transmission matrix $\boldsymbol{T}_{(R,L)}$ with the eigenvalue ηt_p. Similarly, for incidence of the transverse TE beam field $\tilde{\boldsymbol{E}}^{(te)}_{\perp;p,\pm l}$ defined in (35), the same relations are valid with the common eigenvalue t_s :

$$\boldsymbol{T}_{(R,L)}\tilde{\boldsymbol{E}}^{(tm)}_{\perp;p,\pm l} = \eta t_p \tilde{\boldsymbol{E}}^{(tm)}_{\perp;p,\pm l},\ \ \boldsymbol{T}_{(R,L)}\tilde{\boldsymbol{E}}^{(te)}_{\perp;p,\pm l} = t_s \tilde{\boldsymbol{E}}^{(te)}_{\perp;p,\pm l}. \tag{38}$$

The beam fields fulfilled the equation (38) with eigenvalues ηt_p or t_s are called normal modes of the interface [31, 32].

On the other hand, in the transverse polar frame $(\hat{\boldsymbol{e}}_\rho, \hat{\boldsymbol{e}}_\varphi)$, $\rho = \kappa_\perp$ the transmission matrix $\boldsymbol{T} = \boldsymbol{T}_{(\rho,\varphi)}$ is diagonal and reads:

$$\boldsymbol{T}_{(\rho,\varphi)} = \begin{bmatrix} \eta t_p & 0 \\ 0 & t_s \end{bmatrix}. \tag{39}$$

The transverse TM beam field $\tilde{\boldsymbol{E}}^{(tm)}_{\perp;p,\pm l} = \tilde{\boldsymbol{E}}^{(tm)}_{\rho;p,\pm l}$ defined in (33*a*) represents the eigenvector of the matrix $\boldsymbol{T}_{(\rho,\varphi)}$ with the common eigenvalue ηt_p. Similarly, for incidence of the transverse TE beam field $\tilde{\boldsymbol{E}}^{(te)}_{\perp;p,\pm l} = \tilde{\boldsymbol{E}}^{(te)}_{\varphi;p,\pm l}$ defined in (33*b*), the same equation is valid with the eigenvalue t_s:

$$\boldsymbol{T}_{(\rho,\varphi)}\,\tilde{\boldsymbol{E}}^{(tm)}_{\rho;p,\pm l} = \eta t_p \tilde{\boldsymbol{E}}^{(tm)}_{\rho;p,\pm l},\ \ \boldsymbol{T}_{(\rho,\varphi)}\,\tilde{\boldsymbol{E}}^{(te)}_{\varphi;p,\pm l} = t_s \tilde{\boldsymbol{E}}^{(te)}_{\varphi;p,\pm l}. \tag{40}$$

Therefore, it can be stated that the beam fields $\tilde{\boldsymbol{E}}^{(tm)}_{\rho;p,\pm l}$ and $\tilde{\boldsymbol{E}}^{(tm)}_{\varphi;p,\pm l}$ are also normal modes of the interface. Moreover, the beam field given in the transverse polar coordinates $(\hat{\boldsymbol{e}}_\rho, \hat{\boldsymbol{e}}_\varphi)$, $\rho = \kappa_\perp$ or $(\hat{\boldsymbol{e}}_\rho, \hat{\boldsymbol{e}}_\phi)$, $\rho = r_\perp$ in the momentum or configuration domain, respectively, can be obtained on the grounds of (33)–(35) as summation or subtraction of the beam fields given in the transverse circular coordinates $(\hat{\boldsymbol{e}}_R, \hat{\boldsymbol{e}}_L)$ in the momentum domain:

$$\tilde{\boldsymbol{E}}^{(tm)}_{\rho;p,\pm l} = 2^{-1/2}\left(\tilde{\boldsymbol{E}}^{(tm)}_{R;p,\pm l} e^{+i\varphi} + \tilde{\boldsymbol{E}}^{(tm)}_{L;p,\pm l} e^{-i\varphi}\right), \tag{41a}$$

$$\tilde{\boldsymbol{E}}^{(te)}_{\varphi;p,\pm l} = 2^{-1/2} i\left(\tilde{\boldsymbol{E}}^{(te)}_{R;p,\pm l} e^{+i\varphi} - \tilde{\boldsymbol{E}}^{(te)}_{L;p,\pm l} e^{-i\varphi}\right) \tag{41b}$$

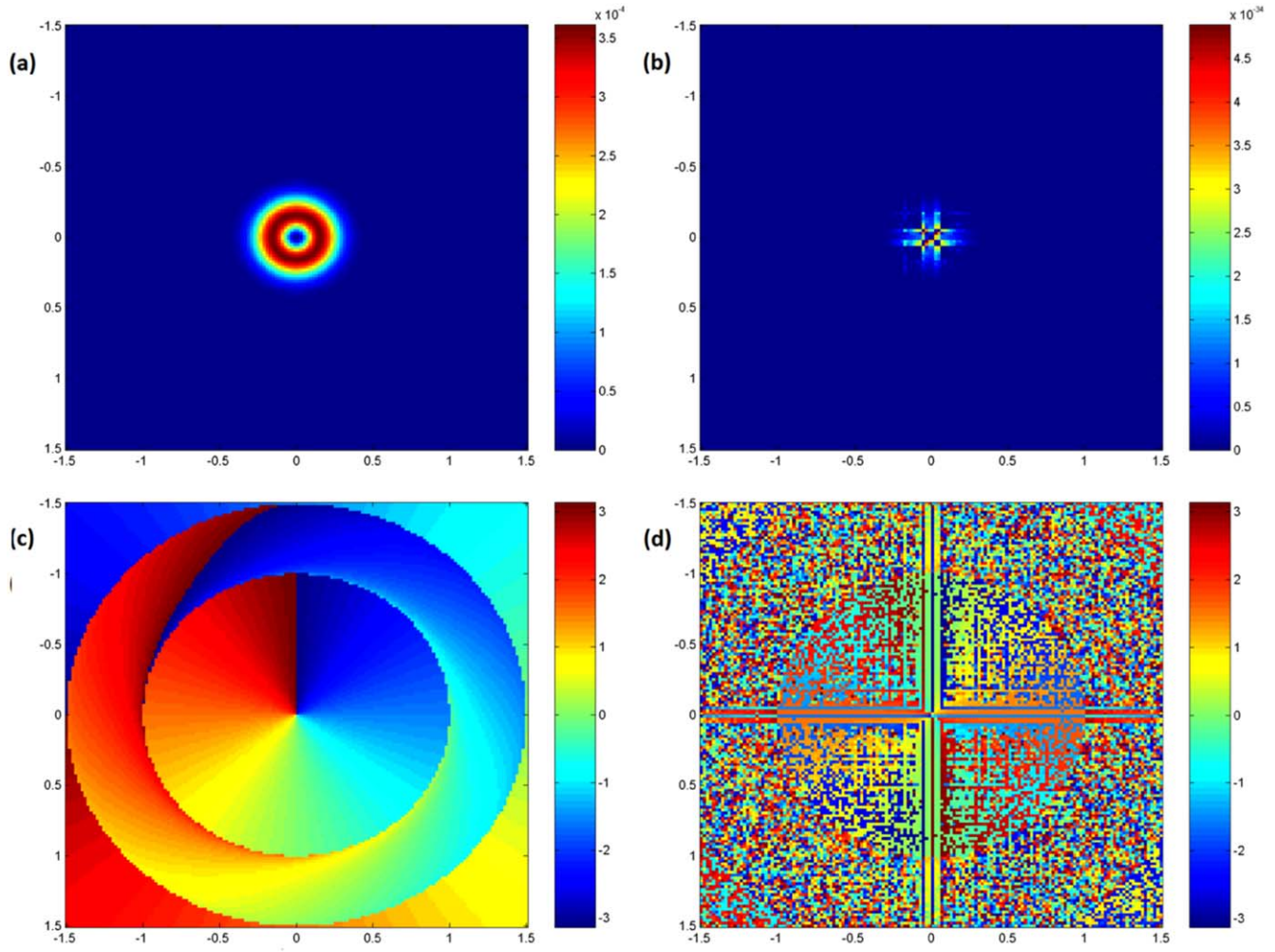

Figure 3. Intensities (a), (b) and phases (c), (d) of beam fields excited at the interface of radial polarization in (a), (c) and of azimuthal polarization in (b), (d). Normal incidence of the beam $\hat{\boldsymbol{e}}_{\rho}\tilde{G}_{0,1}$ of radial polarization, fields shown in the momentum domain in the frame (k_x, k_y).

and in the configuration domain:

$$\boldsymbol{E}^{(tm)}_{\rho;p,\pm l} = 2^{-1/2}\left(\boldsymbol{E}^{(tm)}_{R;p,\pm l}e^{+i\phi} + \boldsymbol{E}^{(tm)}_{L;p,\pm l}e^{-i\phi}\right), \tag{42a}$$

$$\boldsymbol{E}^{(te)}_{\phi;p,\pm l} = 2^{-1/2}i\left(\boldsymbol{E}^{(te)}_{R;p,\pm l}e^{+i\phi} - \boldsymbol{E}^{(te)}_{L;p,\pm l}e^{-i\phi}\right). \tag{42b}$$

In other words, the beam fields of polar polarization fulfilled equation (40) are composed of the beam fields of the circular polarization fulfilled equation (38). One example of such composition is presented in figures 3 and 4. The beam fields are shown in the momentum domain for the incident beams $\hat{\boldsymbol{e}}_{\rho}\tilde{G}_{0,1}$ and $\hat{\boldsymbol{e}}_{\varphi}\tilde{G}_{0,1}$ of radial and azimuthal polarization, respectively.

Note that in figure 3(b) the amplitude of the eLG beam $\hat{\boldsymbol{e}}_{\varphi}\tilde{G}_{0,1}$ is less than 5×10^{-34}. Thus, it approximates zero field in the momentum domain in a quite high precision. This numerical approximation of zero corresponds to the exact zero field component indicated by the upper non-diagonal corner of the transmission matrix $\boldsymbol{T}_{(\rho,\varphi)}$ defined in (39). Moreover, the speckle pattern vivid in figure 3(d) corresponds to the same zero field component. It seems that this purely numerical effect is reminiscent of speckle patterns formed during light propagation through disordered multiply scattering media [30]. Figure 3 shows that, for incidence of the beam $\hat{\boldsymbol{e}}_{\rho}\tilde{G}_{0,1}$ of radial polarization, no beam $\hat{\boldsymbol{e}}_{\varphi}\tilde{G}_{0,1}$ of the orthogonal, azimuthal polarization is excited at the interface. Similarly, as is seen in figure 4, for incidence of the beam $\hat{\boldsymbol{e}}_{\varphi}\tilde{G}_{0,1}$ of azimuthal polarization, no beam $\hat{\boldsymbol{e}}_{\rho}\tilde{G}_{0,1}$ of orthogonal, radial polarization is excited at the interface. Its absence is indicated by zero placed in the lower non-diagonal corner of $\boldsymbol{T}_{(\rho,\varphi)}$. Results of the numerical simulations of the beam fields shown in figures 3 and 4 uniquely confirm the diagonal form of the transmission matrix $\boldsymbol{T}_{(\rho,\varphi)}$ (39) with its eigenvectors $\hat{\boldsymbol{e}}_{\rho}\tilde{G}_{0,1}$ and $\hat{\boldsymbol{e}}_{\varphi}\tilde{G}_{0,1}$.

The discussion presented in this section indicates that the numerical simulations eLG beam interactions with the dielectric interface confirm closely theoretical predictions based on the equations (14)–(19) and (36)–(42). These predictions are valid not only for normal incidence of the eLG beams, but also for their oblique incidence including the cases of Brewster, critical and grazing incidences. Under oblique incidence many interesting phenomena triggered by the cross-polarization coupling [31], like beam spatial reshaping, shifting, splitting and switching, appear [32, 38]. Theoretical predictions of this coupling were subsequently followed by additional numerical simulations of beam propagation and refraction phenomena [39, 40]. Analogical results can be also obtained for the exact eLG beams interacting

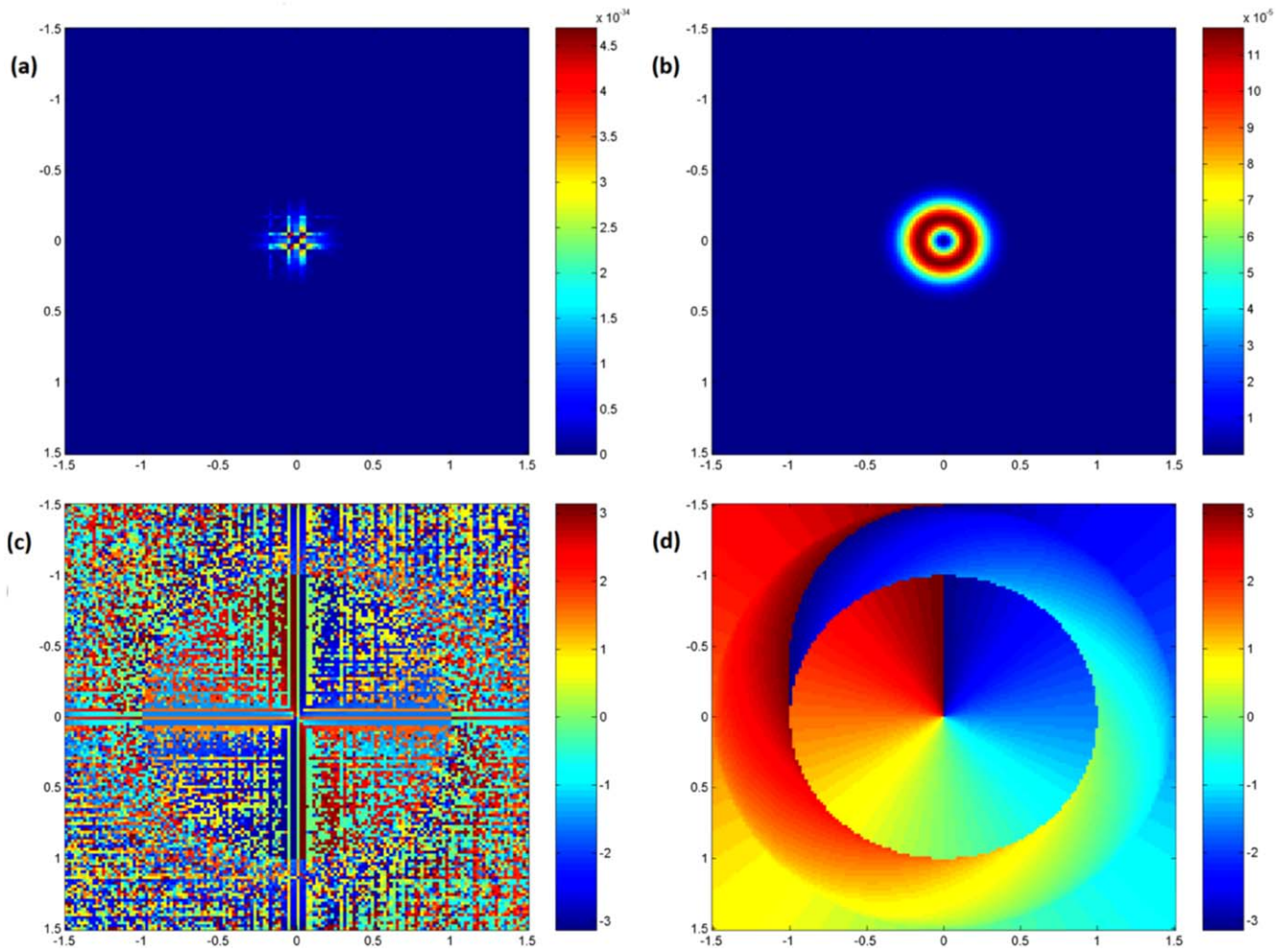

Figure 4. Intensities (a), (b) and phases (c), (d) of beam fields excited at the interface of radial polarization in (a), (c) and of azimuthal polarization in (b), (d). Normal incidence of the beam $\hat{\boldsymbol{e}}_{\varphi}\tilde{G}_{0,1}$ of azimuthal polarization, fields shown in the momentum domain in the frame (k_x, k_y).

with any planar layered dielectric structure, provided that the transmission coefficients specific for such the structure are used in the equations (36), (38)–(40).

8. Conclusions

Scalar and vector representations of exact eLG solutions are presented. The solutions of both types are given in a form of normal modes for free-space beam propagation as well as for beam propagation in stratified media. Transverse TM and TE field components of the vector solution are composed of two still exact parts—paraxial and nonparaxial—distinguished in their amplitudes by the factors f^{-1} and f^{+1}, respectively, where the paraxial parameter f is the ratio between transverse and longitudinal scale parameters of the beams. Total field of the exact solution is defined, in spite of the additional vortex factor, by three independent scalar eLG beams being exact solutions of Helmholtz and Fock equations. At phase front planes of the vector solution, the paraxial and nonparaxial parts of the eLG beams replicate in their form the beam solutions known from conventional approximate analysis. It seems that the presented solution could be useful in analyses of narrow beam interactions with horizontally patterned photonic structures, especially with metasurfaces, metalenses and other components of flat optics [41–46].

Acknowledgments

This work was supported by National Science Centre, Poland, under Grant No. 2015/19/B/ST7/03656.

ORCID iDs

Wojciech Nasalski https://orcid.org/0000-0003-1457-7989

References

[1] Siegman E 1973 Hermite–Gaussian functions of complex argument as optical-beam eigenfunctions *J. Opt. Soc. Am.* **63** 1093–4
[2] Siegman E 1986 *Lasers* (Mill Valley, CA: University Science)

[3] Takenaka T, Yokota M and Fukumitsu O 1985 Propagation of light beams beyond the paraxial approximation *J. Opt. Soc. Am.* A **2** 826–9

[4] Zauderer E 1986 Complex argument Hermite–Gaussian and Laguerre–Gaussian beams *J. Opt. Soc. Am.* A **3** 465–9

[5] Allen L, Padgett M J and Babiker M 1999 The orbital angular momentum of light *Prog. Opt.* **39** 291–372

[6] Padgett M J 2017 Orbital angular momentum 25 years on *Opt. Express* **25** 11265–74

[7] Zhou G and Ru G 2013 Orbital angular momentum density of an elegant Laguerre–Gaussian beam *Prog. Electromagn. Res.* **141** 751–68

[8] Alpmann C, Schöler C and Denz C 2015 Elegant Gaussian beams for enhanced optical manipulation *Appl. Phys. Lett.* **106** 241102

[9] Sheppard J R and Saghafi S 1998 Beam modes beyond the paraxial approximation: a scalar treatment *Phys. Rev.* A **57** 2971–9

[10] Seshadri S R 2002 Virtual source for a Laguerre–Gauss beam *Opt. Lett.* **27** 1872–4

[11] Rodriguez-Morales G and Chavez-Cerda S 2004 Exact nonparaxial beams of the scalar Helmholtz equation *Opt. Lett.* **29** 430–2

[12] Bandres M A and Gutierrez-Vega J C 2004 Higher-order complex source for elegant Laguerre–Gaussian waves *Opt. Lett.* **29** 2213–5

[13] April A 2008 Nonparaxial elegant Laguerre–Gaussian beams *Opt. Lett.* **33** 1392–4

[14] Lee H and Mok J 2014 Spin annihilations of and spin sifters for transverse electric and transverse magnetic waves in co- and counter-rotations *Beilstein J. Nanotechnol.* **5** 1887–98

[15] Barnett S M and Allen L 1994 Orbital angular momentum and nonparaxial light beams *Opt. Commun.* **110** 670–8

[16] Bouchal Z and Olivik M 1995 Non-diffractive vector Bessel beams *J. Mod. Opt.* **42** 1555–66

[17] Volke-Sepulveda K, Garcés-Chávez V, Chávez-Cedra S, Arlt J and Dholakia K 2002 Orbital angular momentum of a high-order Bessel light beam *J. Opt. B: Quantum Semiclass. Opt.* **4** S82–9

[18] Ciattoni A, Conti C and Di Porto P 2004 Vector electromagnetic X waves *Phys. Rev.* E **69** 036608

[19] Ornigotti M, Conti C and Szameit A 2015 Effect of angular momentum on nondiffracting ultrashort optical pulses *Phys. Rev. Lett.* **115** 100401

[20] Belanger P A 1984 Packetlike solutions of the homogeneous-wave equation *J. Opt. Soc. Am.* A **1** 723–4

[21] Sezginer A 1985 A general formulation of focus wave modes *J. Appl. Phys.* **57** 678–83

[22] Ziolkowski R W 1985 Exact solutions of the wave equation with complex source locations *J. Math. Phys.* **26** 861–3

[23] Hillion P 1986 More on focus wave modes in Maxwell equations *J. Appl. Phys.* **60** 2981–2

[24] Ziolkowski R W 1989 Localized transmission of electromagnetic energy *Phys. Rev.* A **39** 2005–33

[25] Besieris I, Abdel-Rahman M, Saharawi A and Chatzipetros A 1998 Two fundamental representations of localized pulse solutions to the scalar wave equation *Prog. Electromagn. Res.* **19** 1–48

[26] Soukoulis C M and Wegener M 2011 Past achievements and future challenges in the development of three-dimensional photonic metamaterials *Nat. Photon.* **5** 523–30

[27] Karimi E, Piccirillo B, Marrucci L and Santamato E 2009 Light propagation in a birefringent plate with topological charge *Opt. Lett.* **8** 1225–7

[28] Maurer C, Jesacher A, Fürhapter S, Bernet S and Ritsch-Marte M 2009 Tailoring of arbitrary optical vector beams *New J. Phys.* **9** 78

[29] Gentilini S, Fratalocchi A, Angelani L, Ruocco G and Conti C 2009 Ultrashort pulse propagation and the Anderson localization *Opt. Lett.* **34** 130–2

[30] McCabe D J, Tajalli A, Austin D R, Bondareff P, Walmsley I A, Gigan S G and Chatel B 2011 Spatio-temporal focusing of an ultrafast pulse through a multiply scattering medium *Nat. Commun.* **2** 447

[31] Nasalski W 2006 Polarization versus spatial characteristics of optical beams at a planar isotropic interface *Phys. Rev.* E **74** 056613

[32] Nasalski W 2010 Cross-polarized normal mode patterns at a dielectric interface *Bull. Pol. Acad. Sci. Tech. Sci.* **58** 141–54

[33] Nasalski W 2013 Exact elegant Laguerre–Gaussian vector wave packets *Opt. Lett.* **38** 809–11

[34] Nasalski W 2014 Vortex and anti-vortex compositions of exact elegant Laguerre–Gaussian beams *Appl. Phys.* B **115** 155–9

[35] Enderlein J and Pampaloni F 2004 Unified operator approach for deriving Hermite–Gaussian and Laguerre–Gaussian laser modes *J. Opt. Soc. Am.* A **21** 1553–8

[36] Bacry H and Cadilhac M 1981 Metaplectic group and Fourier optics *Phys. Rev.* A **23** 2533–6

[37] Stratton J A 1941 *Electromagnetic Theory* (New York: McGraw-Hill)

[38] Nasalski W 2016 Elegant vector Laguerre–Gaussian beams as normal modes at planar photonic structures *EMN Meeting on Quantum Communication and Quantum Imaging—2016* pp 27–8

[39] Szabelak W and Nasalski W 2011 Cross-polarization coupling and switching in an open nano-meta-resonator *J. Phys. B: At. Mol. Opt. Phys.* **44** 215403

[40] Roszkiewicz A and Nasalski W 2014 Optical beam interactions with a periodic array of Fresnel zone plates *J. Phys. B: At. Mol. Opt. Phys.* **47** 165401

[41] Xu T, Agrawal A, Abashin M, Chau K J and Lezec H J 2013 All-angle negative refraction and active flat lensing of ultraviolet light *Nature* **497** 470–4

[42] Lin D, Fan P, Hasman E and Brongersma M L 2014 Dielectric gradient metasurface optical elements *Science* **345** 298–301

[43] Aieta F, Kats M A, Genevet P and Capasso F 2015 Multiwavelenght achromatic metasurfaces by dispersive phase compensation *Science* **347** 1342–5

[44] Khorasaninejad M, Chen W T, Devlin R C, Oh J, Zhu A Y and Capasso F 2016 Metalenses at visible wavelengths: diffraction-limited focusing and subwavelength resolution imaging *Science* **352** 1190–4

[45] Davis J A, Moreno I, Badham K, Sanchez-Lopez M M and Cottrell D M 2016 Nondiffracting vector beams where the charge and the polarization state vary with propagation distance *Opt. Lett.* **41** 2270–3

[46] Makris K G, Brandstötter A, Ambichl P, Musslimani Z H and Rotter S 2017 Wave propagation through disordered media without backscattering and intensity variations *Light Sci. Appl.* **6** e17035